Journal of Solid State Chemistry **166,** 352–361 (2002)
doi:10.1006/jssc.2002.9605

The Crystal Structure of $Ni_{10}Sn_5P_3$

F. J. García-García,* A. K. Larsson,*,[1] and S. Furuseth†

*Arrhenius Laboratory, Department of Inorganic Chemistry, Stockholm University, 106 91 Stockholm, Sweden; and †Department of Chemistry, University of Oslo, N-0315 Oslo 3, Norway

Received November 26, 2001; in revised form March 25, 2002; accepted April 5, 2002

Selected-area electron diffraction revealed that $Ni_{10}Sn_5P_3$ forms a superstructure of the NiAs-type structure. All observed reflections could be fully indexed as $\mathbf{H} = \mathbf{G} + m\mathbf{q}$, where G represents the reflections of the underlying hexagonal *B*8-type average structure, *m* is an integer and $\mathbf{q} = \frac{1}{8}[\bar{3}122]^*$. The resulting space group is $P\bar{1}$ ($Z = 2$). The crystal structure was refined using single-crystal X-ray diffraction methods on a twinned specimen (1651 observed unique reflection, $R_{w\ obs} = 0.0391$). The superstructure reflections are caused by ordering of Sn and P atoms on the hcp array coupled to Ni ordering in $\frac{1}{4}$ of the trigonal bipyramidal sites. The unit-cell parameters refined from powder X-ray diffraction data are $a = 6.419(2)$ Å, $b = 8.322(3)$ Å, $c = 10.278(3)$ Å, $\alpha = 73.32(4)^\circ$, $\beta = 84.41(3)^\circ$, $\gamma = 82.71(2)^\circ$, $V = 520.60(5)$ Å^3. High-resolution electron microscopy images revealed a well-ordered material although macroscopic crystals are twinned. © 2002 Elsevier Science (USA)

Key Words: **Crystal structure; Ni–Sn–P system; $Ni_{10}Sn_5P_3$; Edshammar polyhedron; Superstructure; Twin; Single crystal X-ray diffraction; Selected area electron diffraction; High-resolution electron microscopy.**

INTRODUCTION

NiAs–Ni_2In-type structures ($B8_1$- and $B8_2$- type, respectively) have been studied extensively for the last few decades because of their tremendously diverse range of structural, magnetic and electrical properties (1). The stoichiometry of these compounds can be represented as $T_{1+x}B, 0 \le x \le 1$, where *T* is a transition metal element and *B* is a chalcogen, a pnictide, or a member of the carbon or boron group. When $x = 0$, the structure is of the NiAs-type, where the B atoms form a hexagonal close-packed array and the *T* atoms occupy the octahedra. The resulting space group is $P6_3/mmc$ with *B* atoms in Wyckoff position 2*c* ($\frac{1}{3}\frac{2}{3}\frac{1}{4}$) and *T* atoms in Wyckoff position 2a (000). The Ni_2In type structure ($x = 1$) has the additional *T* atoms in all the trigonal bipyramidal sites (Wyckoff position 2*d* ($\frac{1}{3}\frac{2}{3}\frac{1}{4}$)). The *B*8-type $T_{1+x}B$ phases usually form non-stoichiometric solid solutions in rather wide compositional ranges, in particular at high temperatures where the extra *T* atoms are distributed over the trigonal bipyramidal sites without long-range order. However, the corresponding hexagonal reciprocal lattice is frequently accompanied by varying degrees of highly structured diffuse scattering indicative of short-range order in the filled trigonal bipyramidal sites. At low temperatures, the extra *T* atoms tend to become long-range ordered and this results in superstructure reflections that condense out in reciprocal space (2).

The reciprocal lattice of a modulated *B*8-type structure can be described by $\mathbf{H} = \mathbf{G} + m\mathbf{q}$, where **G** is the set of Bragg reflections from the *B*8-type sublattice, *m* is an integer and **q** is the modulation wave vector (often of the type $[hh\overline{2h}l]^*$ (3–7)). The symmetry of the resultant lattice is often monoclinic or orthorhombic, and the metric distortions away from the original $P6_3/mmc$ *B*8-type sublattice vary greatly among these phases.

Structural analysis in these systems is not easy at all. Single-crystal and/or powder X-ray diffraction data have to be treated with care. Small distortions of the sublattice facilitate merohedral twinning causing an apparently higher symmetry than the true symmetry. Larger distortions of the subcell tend to give rise to large single domains but macroscopic crystals normally show twinned structures along with not fully overlapping sublattices. Further, incommensurate modulations and not well-ordered superstructures are rather common. In this context, a complete characterization of the *B*8-type phases has to be done based on a combination of electron microscopy (electron diffraction and/or high-resolution electron microscopy), single-crystal X-ray diffraction and powder X-ray or neutron diffraction.

Ternary *B*8-type phases with the general formula $T_{1+x}B_{1-y}Pn_y$ (Pn = P, As or Sb) may form structures that are modifications of the known binary $T_{1+x}B$ structures. Studies in such ternary systems are scarce and this article is

[1]To whom correspondence should be addressed. Fax: 011 + 46(0) 8-152187. E-mail: ankie@inorg.su.se.

0022-4596/02 $35.00

part of a work exploring the crystal chemistry of *B*8-type related phases in the Ni–Sn–P system. In the related ternary systems Ni–Ge–P and Ni–Si–P, the crystal structures of the isostructural phases Ni_2SiP (8) and Ni_2GeP (9) have been determined and refined from X-ray diffraction data as have the isostructural phases $Ni_5Si_2P_3$ (10) and $Ni_5Ge_2P_3$ (11). In addition, the reciprocal lattice of $\sim NiGe_{0.2}P_{0.6}$ was explored using electron diffraction and the reciprocal lattice was found to be indicative of an incommensurate displacive modulation of the *B*8-type subcell (12).

Refinement of single-crystal X-ray diffraction data of Ni_2SnP (13) in space group *Pnma* (no. 62, unit-cell parameters $a = 12.8260(7)$ Å, $b = 3.5943(2)$ Å, $c = 5.0896(2)$ Å) showed that Sn and P define a distorted hexagonal close-packed array and all octahedral (and none of the trigonal bipyramidal) sites are occupied with Ni atoms. This structure can be considered as a commensurately modulated structure (superstructure) of the *B*8-type with the modulation wave vector $\frac{1}{4}$ [100]*.

It was previously shown (14) that there is a wide-range non-stoichiometric *B*8-type solid solution field with the general formula $Ni_{1+m}Sn_{1-x}P_x$, $0 \le m \le 0.65$, $0 \le x \le 0.32$. The homogeneity range was found to be strongly temperature dependent. On quenching from 850°C, the *B*8-type was found for a large interval in m and x. For samples quenched from 700°C, the *B*8-type phase field was reduced to two different regions centered around the compositions $\approx Ni_{1.5}Sn_{0.9}P_{0.1}$ ($m = 0.5$ and $x = 0.1$) and $\approx Ni_{1.1}Sn_{0.7}P_{0.3}$ ($m = 0.1$ and $x = 0.3$). Single-crystal X-ray and powder neutron diffraction experiments failed to detect any Sn/P ordering in these *B*8-type phases and it was concluded that both atoms must be randomly distributed in the *B* sites and that the "extra" Ni atoms are partially filling the trigonal bipyramidal sites. However, the large size difference between Sn and P together with the fact that Ni_2SnP is a fully ordered structure (13) suggests that Sn/P ordering is highly likely even though it could not be detected with X-ray diffraction methods. Therefore, a complete electron diffraction study was undertaken (15) which revealed a rather complicated reciprocal space in samples quenched from 850° and a superstructure (referred to here as the α-phase) in samples quenched from 700°. All observed reflections in the reciprocal lattice for the α-phase could be indexed with an expression of the type $\mathbf{G} + m\mathbf{q}$, where $\mathbf{q} = \frac{1}{22}[5\bar{6}15]^*$. This additional scattering to the Bragg reflections of the hexagonal subcell (**G**) strongly supports the idea of Sn/P ordering.

As a result of further studies in the Ni–Sn–P ternary system, we can now report the crystal structure of another commensurate superstructure of the *B*8-type structure; $Ni_{10}Sn_5P_3$ (the β-phase). This new phase was fully characterized by using a combination of X-ray powder and single-crystal diffraction along with the electron microscopy (selected-area electron diffraction, convergent-beam electron diffraction and high-resolution electron microscopy).

EXPERIMENTAL

Samples with nominal composition $Ni_{1.5}Sn_{0.8}P_{0.2}$ were prepared by heating weighed amounts of the elements (Ni: turnings from rods, 99.99%, Johnson, Matthey Laboratory Ltd, Sn: granules, 99.99%, Fluka AG, P: lumps, 99.99%, Koch-Light Laboratories, Ltd.) in evacuated and sealed silica glass ampoules at 800°C for a week. The samples were crushed and annealed, one portion at 700°C for 2 months, and the other at 850°C for 3 weeks. They were then quenched in ice water and analyzed by powder X-ray diffraction using a Guinier–Hägg camera with Cu$K\alpha_1$ radiation and Si as internal standard. The lines were assigned to the individual phases by simulating the pattern with the program PowderCell (16) and the unit-cell parameters were obtained by least-squares refinements using the PIRUM program (17).

The samples for EM were prepared by grinding the specimen under butanol and placing one drop of the resulting suspension onto a holey carbon film supported by a copper grid. For high-resolution electron microscopy experiments, a JEM-3010 UHR microscope operating at 300 kV was used (structural resolution of 1.7 Å and $CS = 0.6$ mm) and a JEM-4000EX microscope operated at 400 kV (structural resolution of 1.8 Å and $CS = 1.2$ mm) equipped with a slow-scan CCD camera (Gatan MSC model 794). Selected-area and convergent-beam electron diffraction experiments were carried out in a JEOL 2000FX microscope operated at 200 kV. This is equipped with a LINK AN10000 analysis system used for energy-dispersive X-ray spectroscopy. Image processing and analysis of high-resolution electron microscopy images were performed with CRISP software (18) and Digital Micrograph (Gatan In. Pleasanton, CA, USA). Image simulations were carried out with the NCEMSS program system (19) using multislice algorithms.

Single-crystal X-ray diffraction data were collected using a STOE image plate system connected to a rotating anode (Siemens M18XHF) with Mo$K\alpha$ radiation. Psi-scans used for absorption correction were recorded using a STOE (AEDZ) diffractometer. Data reduction was performed with the programs X-Shape (20) and X-Red (21), the structure was solved with direct methods (SHELX (22)) while data handling and refinements were performed using JANA2000 (23). The sample was carefully studied in the optical microscope. All the grains were gray metallic and of irregular shape. About 10 grains were selected, mounted on glass rods and tested for single-crystal X-ray experiments by acquiring test series of image plates.

RESULTS

Powder X-Ray Diffraction

Powder X-ray diffraction patterns of the high-temperature (850°C) sample only showed lines that could be indexed as belonging to a hexagonal *B*8-type structure and a few lines from unreacted Sn metal. The unit-cell parameters refined in the $P6_3/mmc$ cell were $a = 3.784(2)$ Å, $c = 5.218(4)$ Å and $V = 64.75$ Å^3.

A plethora of lines was observed in the powder X-ray diffraction patterns of the low-temperature (700°C) samples. By using the results from the electron diffraction and single-crystal X-ray diffraction experiments, the lines could be shown to belong only to $\sim Ni_3Sn_2$, Ni_2SnP and the new phase $Ni_{10}Sn_5P_3$. Twenty-four lines could be uniquely indexed as belonging to $Ni_{10}Sn_5P_3$ which render the refined unit-cell parameters $a = 6.419(2)$ Å, $b = 8.322(3)$ Å, $c = 10.278(3)$ Å, $\alpha = 73.32(4)°$, $\beta = 84.41(3)°$, $\gamma = 82.71(2)°$ and $V = 520.60(5)$ Å^3. For Ni_2SnP, 27 reflections were used to refine the unit-cell parameters resulting in $a = 12.863(7)$ Å, $b = 3.602(2)$ Å, $c = 5.063(3)$ Å, $V = 234.58(9)$ Å^3.

Electron Diffraction

The *B*8-type crystallites in the high-temperature sample showed the same type of strong and highly structured diffuse scattering in addition to the reflections from the underlying *B*8-type substructure as reported by Furuseth *et al.* (15).

Ni_2SnP was found to be present in the low-temperature sample. Symmetry analysis performed with convergent-beam electron diffraction along the major zone axes confirmed symmetry to be of the space group *Pnma* as reported for this phase (13) and the high-resolution electron microscopy studies showed a well-ordered material. Stacking faults in the (001) planes of the parent hexagonal structure could sometimes be detected.

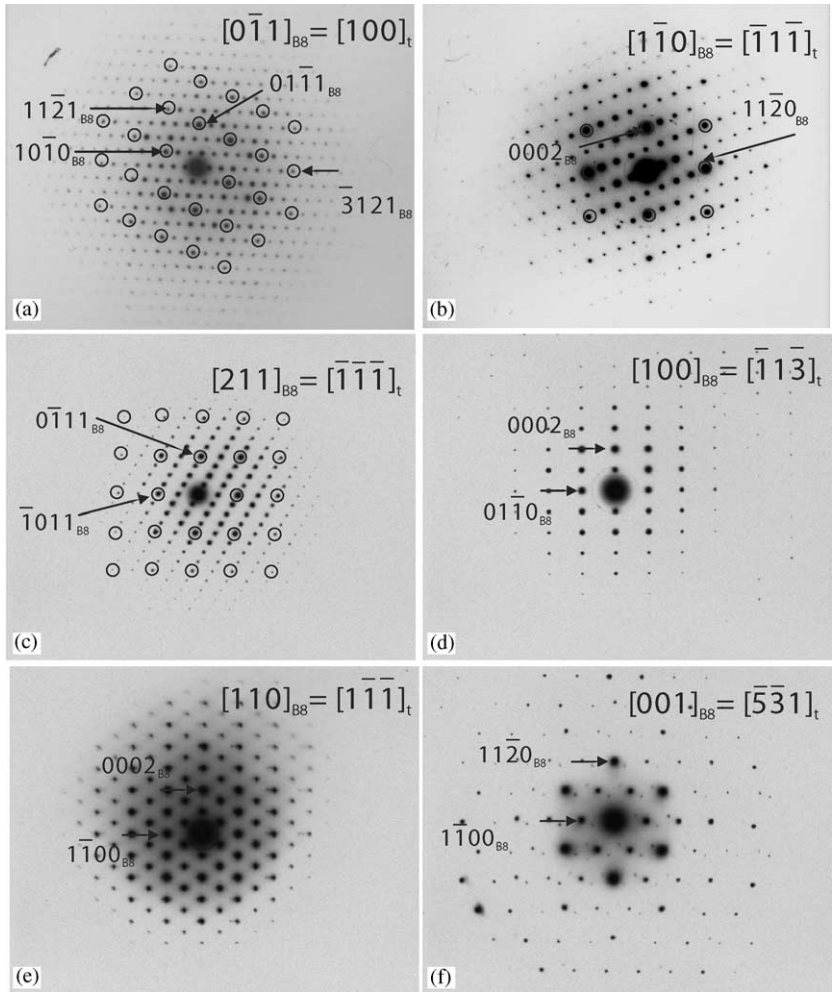

FIG. 1. Typical zone axis electron diffraction patterns (EDPs) of $Ni_{10}Sn_5P_3$ indexed according to the underlying hexagonal *B*8-type structure. The zone axis of the corresponding triclinic cell is also indicated.

$Ni_{10}Sn_5P_3$ was found to be the major component of the low-temperature sample. Detailed tilting experiments were performed keeping the known reciprocal directions of the *B*8-type sublattice excited. In Fig. 1, a series of some typical zone axis electron diffraction patterns (EDPs) is presented. The required expression to index all observed reflections in the reciprocal lattice of $Ni_{10}Sn_5P_3$ is of the type $\mathbf{H} = \mathbf{G} + m\mathbf{q}$, with $\mathbf{q} = \frac{1}{8}[\bar{3}121]^*_{B8}$. Subscripts *B*8 and *t* refer, in what follows, to the parent hexagonal *B*8-type structure and to the triclinic superstructure, respectively.

The presence of this modulation wave vector in the reciprocal space forbids all symmetry elements inherited from the $P6_3/mmc$ space group of the *B*8-type sublattice so that the highest possible resultant space group is $P\bar{1}$. A triclinic reciprocal unit cell can be chosen as $\mathbf{a}^*_t = \frac{1}{8}[\bar{1}3\bar{2}\bar{5}]^*_{B8}$, $\mathbf{b}^*_t = \frac{1}{8}[1\bar{3}2\bar{3}]^*_{B8}$ and $\mathbf{c}^*_t = \mathbf{q} = \frac{1}{8}[\bar{3}121]^*_{B8}$ which corresponds to a real space unit cell with $\mathbf{a_t} = \mathbf{b_{B8}} - \mathbf{c_{B8}}$, $\mathbf{b_t} = -\mathbf{a_{B8}} - 2\mathbf{b_{B8}} - \mathbf{c_{B8}}$ and $\mathbf{c_t} = -3\mathbf{a_{B8}} - \mathbf{b_{B8}}$. The EDPs presented in Fig. 1 are indexed with respect to the underlying hexagonal *B*8-type subcell and the corresponding directions for the triclinic superstructure are also indicated.

Figure 1a shows an EDP along $[0\bar{1}1]_{B8}$ corresponding to $[100]t$. Circled reflections correspond to the hexagonal *B*8-type sublattice. Note that all additional reflections can be indexed with the modulation wave vector $\mathbf{q} = \frac{1}{8}[\bar{3}121]^*_{B8}$. Figure 1b shows the EDP along $[1\bar{1}0]_{B8} = [\bar{1}1\bar{1}]_t$. In this EDP, a modulation wave vector can be chosen as $\mathbf{q}' = \frac{1}{4}[11\bar{2}1]^*_{B8}$ to index all superstructure reflections in the zero-order laue zone (ZOLZ). However, this vector is not sufficient to index the whole set of reflections in the reciprocal lattice of $Ni_{10}Sn_5P_3$. Nevertheless, EDPs recorded along $[1\bar{1}0]_{B8}$ are useful to compare the $Ni_{10}Sn_5P_3$ structure to structure modulations of binary $T_{1+x}BB$8-type phases, where $[hh\overline{2h}l]$* is a common modulation wave direction.

Figures 1d and 1e show EDPs along $[100]_{B8}$ and $[110]_{B8}$, respectively, which are equivalent directions in the *B*8-type sublattice, but independent in the triclinic structure of $Ni_{10}Sn_5P_3$. In Fig. 1d, no part of the superstructure is projected and no extra reflections are visible in ZOLZ; however, to the right of the figure reflections in higher order laue zones (HOLZ) confirm that there is a superstructure in the crystallite. Figure 1f shows the EDP along the $[001]_{B8}$ zone axis. In this projection, as in Fig. 1d, only reflections from the *B*8-type sublattice are excited but reflections from the first-order Laue zone (FOLZ) are visible close to the center due to the very long projection axes of the superstructure. Note that reflections from HOLZ appearing in Fig. 1f break all symmetry from the *B*8-type structure.

The triclinic symmetry is clear from the electron diffraction experiments and the only possible space groups are *P*1 or $P\bar{1}$. Microdiffraction experiments suggested the existence of an inversion center as the projection symmetry was (2) along all studied directions (24). The inversion center was also suggested by crystallographic processing of high-resolution images, see below, and confirmed with the single-crystal X-ray diffraction data refinement.

Single-Crystal Refinements

Image plates from many crystals were studied. All the crystals were twinned and not well suited for single-crystal X-ray experiments. However, one crystal was found in which the reciprocal lattice were composed of only one *B*8-type sublattice with superstructure reflections which could

TABLE 1
Crystal Data and Structure Refinement for $Ni_{10}Sn_5P_3$

Chemical formula	$Ni_{10}Sn_5P_3$
Formula weight (g/mol)	1273.4
Crystal system	Triclinic
Space group	$P\bar{1}$
a (Å)	6.419(2)
b (Å)	8.322(3)
c (Å)	10.278(3)
α (deg)	73.32(4)
β (deg)	84.41(3)
γ (deg)	82.71(2)
V (Å^3)	520.60(5)
D_x (mg m^{-3})	8.045
Z	2
Crystal form	Irregular
Crystal size	$\emptyset \approx 0.5$ mm
Color	Gray metallic
Absorption coefficient (mm^{-1})	29.6
Diffractometer	STOE IPDS
Radiation	Mo$K\alpha$
No. of reflections measured	6305
No. of independent reflections	2887
No. of observed reflections	1651
Observation criterion	$I \leq 3\sigma(I)$
Absorption correction	Numerical from crystal shape
T_{min}, T_{max}	0.2207, 0.4497
$R_{int,all}$	3.971
Range of $h\,k\,l$	$-7 \rightarrow h \rightarrow 7$ $-8 \rightarrow k \rightarrow 9$ $0 \rightarrow l \rightarrow 11$
Temperature	25°C
Refinements on	F All independent measured
No. of parameters refined	No. of reflections used in refinements
Weighting scheme	$\varpi = 1/\sigma^2$
R_{obs}	4.49
wR_{obs}	3.91
R_{all}	10.87
wR_{all}	4.35
S_{all}	5.05
$(\delta/\sigma)_{max}$	0.0004
$\Delta\rho_{max}$(e Å^{-3}), $\Delta\rho_{min}$(e Å^{-3})	3.62, −2.95
Source of atomic-scattering factors	International tables for X-ray crystallography (1974, Vol. IV)

be described with the vectors $\mathbf{q}_1 = \frac{1}{8}[\bar{3}121]^*_{B8}$ and $\mathbf{q}_2 = \frac{1}{8}[21\bar{3}1]^*_{B8}$. The metrical distortions of the sublattice away from the hexagonal *B*8-type lattice are quite large and result in a metrically close to orthorhombic sublattice with $\mathbf{a_{ort}} = -\mathbf{b_{B8}}$, $\mathbf{b_{ort}} = 2\mathbf{a_{B8}} + \mathbf{b_{B8}}$ and $\mathbf{c_{ort}} = \mathbf{c_{B8}}$. This orthorhombic sublattice is common for the two twins represented with $\mathbf{q_1}$ and $\mathbf{q_2}$, respectively, in the reciprocal space. Thus, reflection data for both twins could be integrated simultaneously in an orthorhombic twin cell (tc) with $a_{tc} = 8a_{ort} = 29.54$ Å, $b_{tc} = 8b_{ort} = 54.22$ Å and $c_{tc} = 8c_{ort} = 41.93$ Å. This diffraction data set was corrected for absorption using the shape of the crystal as optimized by 16 psi-scans and the data set was then decomposed: The twin 1 reflections were selected as reflections compatible with the cell $\mathbf{a_t} = -\frac{1}{8}\mathbf{c_{tc}}$, $\mathbf{b_t} = -\frac{3}{16}\mathbf{a_{tc}} - \frac{1}{16}\mathbf{b_{tc}} - \frac{1}{8}\mathbf{c_{tc}}$ and $\mathbf{c_{tc}} = -\frac{1}{16}\mathbf{a_{tc}} - \frac{3}{16}\mathbf{b_{tc}}$. The reflections from twin 2 was selected by the twin matrix representing $\mathbf{a}_2 = \mathbf{a_t}, \mathbf{b}_2 = -\frac{1}{8}\mathbf{a_t} - \frac{7}{8}\mathbf{b_t} - \frac{5}{8}\mathbf{c_t}$ and $\mathbf{c}_2 = -\frac{3}{8}\mathbf{a_t} + \frac{3}{8}\mathbf{b_t} - \frac{7}{8}\mathbf{c_t}$.

Twin 1 scattering dominated the data set and the structure could be solved using data from this twin only. The preliminary refinements were also performed using only data from twin 1; when only isotropic temperature parameters were applied 71 refined parameters using 1542 reflections (1185 observed) gave the residual values $R_{obs} = 3.91$, $R_{w\,obs} = 4.00$, $R_{all} = 5.10$ and $R_{w\,all} = 4.01$. Refinement of anisotropic temperature parameters resulted in four atoms (P1–P3 and Sn2) with negative-definite temperature parameters indicating an unsatisfactory refinement. This was because the scattering power of twin 2 contributing to the set of reflections from the *B*8-type sublattice (**G**) was not taken into account at this step. The quality of the refinements was improved when all of the reflections from both twins were included. One hundred and sixty-eight parameters, refined using 2885 reflections (1651 observed) gave the residual values $R_{obs} = 4.49$, $R_{w\,obs} = 3.91$, $R_{all} = 10.87$ and $R_{w\,all} = 4.35$. Even if this final refinement has higher residual values than the preliminary refinement with only twin 1, the refined parameters from the final refinement are more reliable. The volume ratio of twin 2 obtained from the refinements was 12%, which is in agreement with the inspection of the diffraction data. A detailed description of the crystal data, data acquisition and refinement is found in Table 1 and final atomic coordinates and the refined isotropic temperature parameter are listed in Table 2. Central–apex distances in the coordination polyhedra around all the atoms in the structure are given in Table 3.

Description of the Structure

In $Ni_{10}Sn_5P_3$, Sn and P form a distorted hexagonal close-packed array with all the octahedral sites occupied by Ni atoms (Ni1–Ni9 or Ni_{oct}). One-quarter of the trigonal bipyramidal sites are also occupied by Ni atoms (Ni10 and Ni11). The structure can be described based on the *B*8-type structure and in Fig. 2a a sketch of an octahedra $(001)_{B8}$ layer is drawn. In such a layer, Sn and P define the vertices of the octahedra that are all filled with Ni_{oct} atoms. The positions of the extra Ni atoms in trigonal bipyramids, Ni10 and Ni11, are indicated by dark gray spheres. The P atoms are situated in such a way that they form isolated triangles in the sheet. The triangles of P atoms are indicated by black lines. Note that the Ni10 and Ni11 atoms in the trigonal bipyramids are capping two of the sides of the

TABLE 2
Fractional Atomic Coordinates and Thermal Displacement Parameters for $Ni_{10}Sn_5P_3$

Atoms	*x*	*y*	*z*	U_{iso} (Å2)	x_{und}	y_{und}	z_{und}
Sn1	0.03308(9)	0.18426(8)	−0.62717(7)	0.0090(2)	0.0729	0.1771	−0.6146
Sn2	−0.29891(9)	0.55129(9)	−0.74073(8)	0.0103(2)	−0.3021	0.5529	−0.7396
Sn3	0.35218(9)	−0.08915(9)	0.13146(7)	0.0098(2)	0.3229	−0.0729	0.1354
Sn4	0.20865(9)	0.04934(9)	−0.24089(8)	0.0102(2)	0.1979	0.0521	−0.2396
Sn5	−0.53563(9)	0.81852(8)	−0.49613(7)	0.0099(2)	−0.5521	0.8021	−0.4896
P1	−0.0774(4)	0.2777(3)	0.0173(3)	0.0144(9)	−0.0521	0.3021	0.0104
P2	0.6111(3)	−0.3144(4)	−0.1124(3)	0.0150(9)	0.5729	−0.3229	−0.1146
P3	−0.1981(3)	0.4055(3)	−0.4006(3)	0.0123(9)	−0.1771	0.4271	−0.3646
Ni1	0.4184(2)	0.0817(2)	0.2938(1)	0.0093(4)	0.4375	0.0625	0.3125
Ni2	−0.1348(2)	0.1335(2)	−1.3752(2)	0.0079(4)	−0.1250	0.1250	−1.3750
Ni3	0	0	0	0.0104(6)	0	0	0
Ni4	−0.5	0.5	−0.5	0.0075(6)	−0.5	0.5	−0.5
Ni5	0.2700(2)	0.2113(2)	−0.0390(1)	0.0126(5)	0.3125	0.1875	−0.0625
Ni6	−0.7111(2)	0.7272(2)	−0.2024(1)	0.0105(4)	−0.75	0.75	−0.25
Ni7	0.1464(2)	0.3488(2)	−0.4511(1)	0.0093(4)	0.1875	0.3125	−0.4375
Ni8	−0.3983(2)	0.3925(2)	−0.0706(1)	0.0094(4)	−0.3750	−0.3750	−0.1250
Ni9	0.9456(2)	−0.4322(2)	−0.1285(1)	0.0116(4)	0.9375	−0.4375	−0.1875
Ni10	−0.0563(2)	0.2961(2)	−1.2032(1)	0.0107(4)	−0.0104	0.2604	−1.1979
Ni11	−0.3412(2)	0.6036(2)	−0.3064(1)	0.0097(4)	−0.3840	0.6340	−0.3210

TABLE 3
Central–Apex Distances (Å) in the Coordination Polyhedra around the Atoms

Ni1	Ni2	Ni3	Ni4	
Sn1 2.645(1)	Sn1 2.643(2)	Sn3 2.6645(6) (× 2)	Sn2 2.6229(7) (× 2)	
Sn3 2.576(2)	Sn1 2.635(2)	Sn4 2.6458(7) (× 2)	Sn5 2.6407(7) (× 2)	
Sn4 2.580(1)	Sn3 2.697(2)	P1 2.353(3) (× 2)	P3 2.230(2) (× 2)	
Sn5 2.605(1)	Sn4 2.631(1)	Ni5 2.546(1) (× 2)	Ni7 2.670(1) (× 2)	
Sn5 2.651(2)	Sn5 2.535(2)	Ni10 2.743(1) (× 2)	Ni11 2.709(2) (× 2)	
P2 2.272(3)	P3 2.191(3)			
Ni2 2.624(2)	Ni1 2.624(2)			
Ni6 2.548(2)	Ni7 2.610(2)			
Ni11 2.639(2)	Ni10 2.631(2)			
Ni5	**Ni6**	**Ni7**	**Ni8**	**Ni9**
Sn2 2.549(1)	Sn1 2.734(1)	Sn1 2.757(2)	Sn2 2.785(2)	Sn1 2.758(1)
Sn3 2.631(1)	Sn2 2.537(2)	Sn2 2.657(2)	Sn3 2.743(2)	Sn2 2.747(1)
Sn3 2.704(1)	Sn4 2.585(2)	Sn4 2.803(1)	P1 2.314(3)	P1 2.461(3)
P1 2.290(3)	Sn5 3.031(2)	Sn5 2.790(1)	P2 2.357(3)	P1 2.231(4)
Sn4 2.858(2)	P1 2.221(3)	P3 2.247(2)	P2 2.201(3)	P2 2.259(3)
P2 2.214(4)	P2 2.297(3)	P3 2.211(3)	Ni5 2.704(2)	P2 2.259(3)
Ni3 2.546(1)	Ni1 2.548(2)	Ni2 2.610(2)	Ni6 2.822(2)	Ni5 2.993(2)
Ni8 2.704(2)	Ni8 2.822(2)	Ni4 2.670(1)	Ni8 2.746(2)	Ni6 2.652(2)
Ni9 2.993(2)	Ni9 2.652(2)	Ni7 2.933(2)	Ni9 2.724(2)	Ni8 2.724(2)
Ni10 2.717(2)	Ni11 2.715(2)	Ni10 2.690(2)	Ni10 2.633(2)	Ni8 2.724(2)
		Ni11 2.623(2)	Ni11 2.576(2)	Ni9 2.681(2)
				Ni10 2.588(2)
				Ni11 2.653(2)
Ni10	**Ni11**	**P1**	**P2**	**P3**
Sn2 2.684(1)	Sn1 2.724(1)	Ni3 2.353(3)	Ni1 2.272(3)	Ni2 2.191(3)
Sn3 2.635(1)	Sn2 2.723(1)	Ni5 2.290(3)	Ni5 2.214(4)	Ni4 2.230(2
Sn4 2.590(1)	Sn5 2.544(1)	Ni6 2.221(3)	Ni6 2.297(3)	Ni7 2.247(2)
P1 2.218(3)	P2 2.268(4)	Ni8 2.314(3)	Ni8 2.357(3)	Ni7 2.211(3)
P3 2.205(3)	P3 2.203(3)	Ni9 2.461(3)	Ni8 2.201(3)	Ni10 2.205(3)
Ni2 2.631(2)	Ni1 2.639(2)	Ni9 2.231(4)	Ni9 2.259(3)	Ni11 2.203(3)
Ni3 2.743(1)	Ni4 2.709(2)	Ni10 2.218(3)	Ni11 2.268(4)	
Ni5 2.717(2)	Ni6 2.715(2)			
Ni7 2.690(2)	Ni7 2.623(2)			
Ni8 2.633(2)	Ni8 2.576(2)			
Ni9 2.588(2)	Ni9 2.653(2)			
Ni11 2.943(2)				

triangle formed by P atoms. This layer is denoted as 0 in the picture. The Ni10 and Ni11 positions and the corresponding P triangle one layer up are indicated with bigger light gray spheres and broken black lines, respectively. The same motifs as those marked in layers 0 and 1 are found again at the positions marked with 2 and 3, respectively, corresponding to 2 and 3 octahedral layers up. The structural motif is hence stacked along $[0\bar{1}1]_{B8}$, which corresponds to $[100]_t$.

The arrows at the top of the figure indicate every fourth $[1\bar{1}0]_{B8}$ row of trigonal bipyramidal sites in the plane. This is to demonstrate the relationship between $Ni_{10}Sn_5P_3$ and most binary superstructures of the *B*8-type structure where such rows are either totally empty or totally filled with additional *T* atoms; in $Ni_{10}Sn_5P_3$, only every second trigonal bipyramidal position are filled along the rows since the structure motif here is more complex.

The atoms coordinating Ni10 and Ni11 (see Table 3) define the 11-vertex polyhedra referred to as Edshammar polyhedra (25, 26) (E10 and E11, respectively). An Edshammar polyhedron consists of a trigonal prism (here $6Ni_{oct}$) and a trigonal bipyramid (here 3Sn + 2P) merged together to form an 11-vertex polyhedron. The two P atoms are at the base of the trigonal bipyramids. E10 and E11 are very similar and share a face built up by Ni8, Ni9 and P3 as shown in Fig. 2b where the pair of Edshammar polyhedra are drawn roughly perpendicular to the $[001]_{B8}$ projection of Fig. 2a. The interatomic distances in E10 and

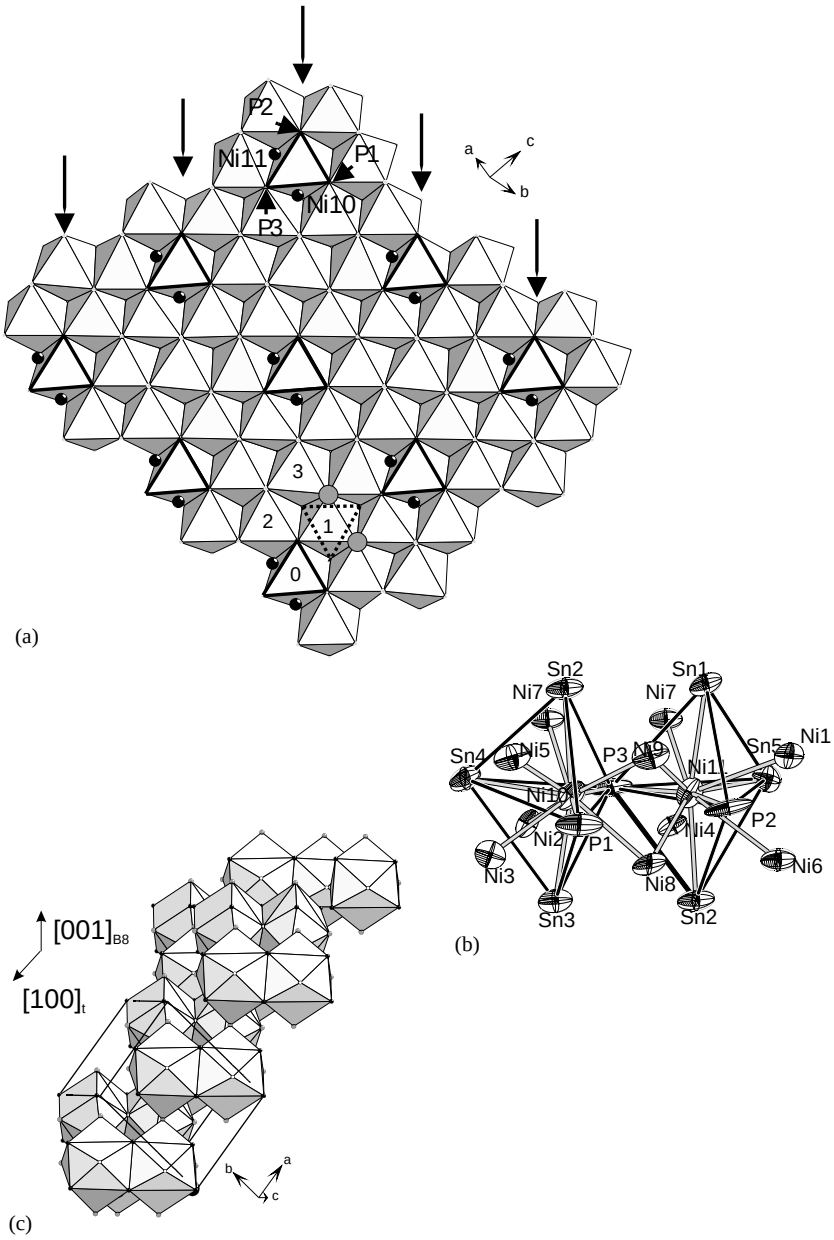

FIG. 2. (a) A sheet of octahedra showing the hcp layer of Sn/P atoms in $Ni_{10}Sn_5P_3$. The P atoms form triangles which are outlined. Ni10 and Ni11 which are capping this triangle are also indicated. In the bottom part, the position of the capped triangle in successive layers is indicated. Odd and even layers are each others inversion and identical layers are stacked along $[100]_t = [0\bar{1}1]_{B8}$. (b) The face-sharing Edshammar polyhedra of Ni_{okt}, Sn and P coordinating Ni10 and Ni11 viewed perpendicular to $[001]_{B8}$. Anisotropic displacements (99% probability) are shown. (c) A larger portion of the structure along the same direction as b) but with the Edshammar polyhedra outlined. The triclinic unit cell is outlined. Note how the Edshammar polyhedra share corners along $[100]_t$.

E11 are similar and the central Ni10 and Ni11 atoms are both shifted towards the P atoms creating Ni10,11–P distances of 2.20–2.27 Å and Ni10,11–Sn distances of 2.54–2.72 Å. The Ni10,11–Ni_{okt} distances are all between 2.58 and 2.74 Å (see Table 3).

This pair of face-sharing Edshammar polyhedra can be used as the building unit to describe the structure. Figure 2c shows a larger portion of the structure along the same direction as in Fig. 2b but with the Edshammar polyhedra outlined. The crystal structure of $Ni_{10}Sn_5P_3$ can be described as built up of corner-connected units of such pairs of face-sharing Edshammar polyhedra.

The Edshammar pairs share corners along $[0\bar{1}1]_{B8} = [100]_t$. In Fig. 3, the structure is projected along these rows

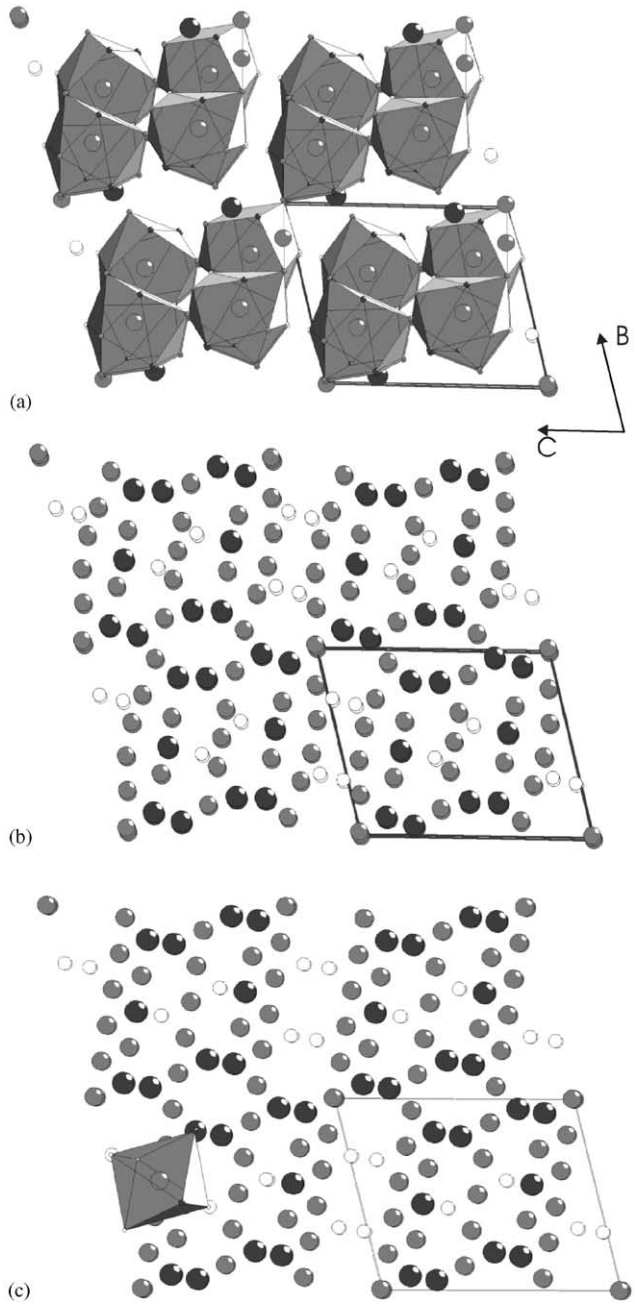

FIG. 3. The same portion of the structure as in Fig. 2c but projected along the string of corner-sharing Edshammar polyhedra. This is the same $[100]_t = [0\bar{1}1]_{B8}$ projection direction as for the EDP in Fig. 1a which is the best projection for high-resolution electron microscopy imaging. (a) The Edshammar polyhedra are outlined. (b) The atomic positions are outlined; large black disks represent Sn, medium gray represents Ni and small white represents P. Compare the atomic positions with the atomic sites in (c), where the atomic positions are unshifted with respect to the *B*8 substructure.

of corner-sharing Edshammar pairs; Fig. 3a demonstrates how the rows of Edshammar polyhedra are connected to double chains by E10–E10 and E10–E11 corner sharing. These double chains are linked via E11–E11 corner sharing along $[1\bar{1}0]_t$. Along this $[0\bar{1}1]_{B8} = [100]_t$ projection, atomic columns are composed of the same type of atoms and this projection is the most useful one for structural imaging using high-resolution electron microscopy (vide infra). In Fig. 3b, only the positions of the atoms are indicated and in Fig. 3c the positions of the atoms in an undistorted *B*8 array are shown for comparison. All Sn atoms and P1 and P2 are rather close to the ideal positions while P3, Ni8 and Ni9 have the largest shifts compared to the ideal positions in a *B*8-type structure.

The coordination polyhedra around P1 and P2 are trigonal prisms of Ni_{okt} monocapped by Ni10 and Ni11, respectively, with P–Ni distances between 2.20 and 2.46 Å (Figs. 4a and 4b). Also, P3 is coordinated by a trigonal prism of Ni atoms, and this is interesting as it is *not* formed from the $6T_{okt}$ atoms forming the trigonal prism surrounding the *B* atoms in a *B*8-type structure. Figure 4c shows how two of the Ni_{okt} atoms (Ni8 and Ni9) are shifted away from the P3 atom and the trigonal prism is instead formed from four of the Ni_{okt} atoms and Ni10 and Ni11. This trigonal prism is very regular and all P3–Ni distances are within the range 2.19–2.25 Å.

Sn2 is coordinated by a trigonal prism of Ni_{okt} atoms capped by both Ni10 and Ni11 while Sn1, Sn3 and Sn4 are coordinated by a monocapped (Ni10 or Ni11) trigonal prism of Ni_{okt}. In the monocapped prism around Sn5, Ni6 is pulled away so that the coordination is more accurately described as $6+1$.

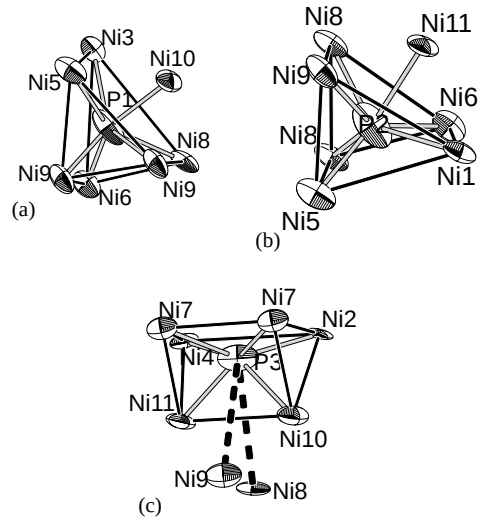

FIG. 4. Coordination polyhedra around (a) P1, (b) P2 and (c) P3 oriented roughly along $[001]_{B8}$. Note that the trigonal prism around P3 is tilted 90° with respect to the trigonal prisms of P1 and P2 which are inherited directly from the *B*8-type substructure; only four Ni_{okt} atoms are however coordinating P3. Ni8 and Ni9 are shifted away (compared to the substructure) and instead Ni10 and Ni11 are shifted towards P3 to complete the trigonal prism. Anisotropic displacements (99% probability) are shown.

Ni1–Ni5 and Ni7 are coordinated by 6 *B* atoms (Sn + P) in the distorted octahedra and 3–4 Ni atoms while for Ni6, Ni8 and Ni9, only five of the *B* atoms are close enough to belong to the coordination polyhedron.

Symmetry distortions of the *B*8-type structure have been described in MnP and NiP (27), where interaction between neighboring phosphorous atoms give rise to phosphorous chains $d_{P-P} = 2.81$ Å (MnP) and phosphorous pairs $d_{P-P} = 2.43$ Å (NiP). Such P–P interactions are not present in $Ni_{10}Sn_5P_3$ where the shortest P–P distance is $d_{P1-P2} = 3.29$ Å (or in Ni_2SnP where the P–P distances are about 3.57 Å).

High-Resolution Electron Microscopy

High-resolution electron microscopy images were recorded along the major zone axis of the $Ni_{10}Sn_5P_3$ crystals. The phase was stable under the electron beam and the crystals had a well-ordered microstructure with very few defects. No domain twinning was detected. The projection symmetry of the experimental images was evaluated by applying symmetrization to the amplitudes and phases of the peaks obtained by fast Fourier transform of the experimental images. The values for the residual phase indicate the planar group *p*2 as the most possible one in agreement with the results forming the single-crystal X-ray diffraction refinements and the electron diffraction studies.

In Fig. 5a, a high-resolution electron microscopy image along $[0\bar{1}1]_{B8} = [100]_t$ of $Ni_{10}Sn_5P_3$ is shown. In Fig. 5b, a filtered, averaged and enlarged area of the thinnest part of the crystal is shown. This image was obtained by masking the Bragg reflections in the Fourier transform of the original image (Fig. 5c) and then performing an inverse Fourier transform. A simulated image of $Ni_{10}Sn_5P_3$ is given as inset. The experimental image was recorded at 400 kV and acquired with a slow scan CCD camera. The inset image was simulated with a defocus of −450 Å and thickness of 20 Å using multislice algorithms.

CONCLUSIONS

The crystal structure of $Ni_{10}Sn_5P_3$ is a new type of superstructure related to the *B*8-type structure. The super-

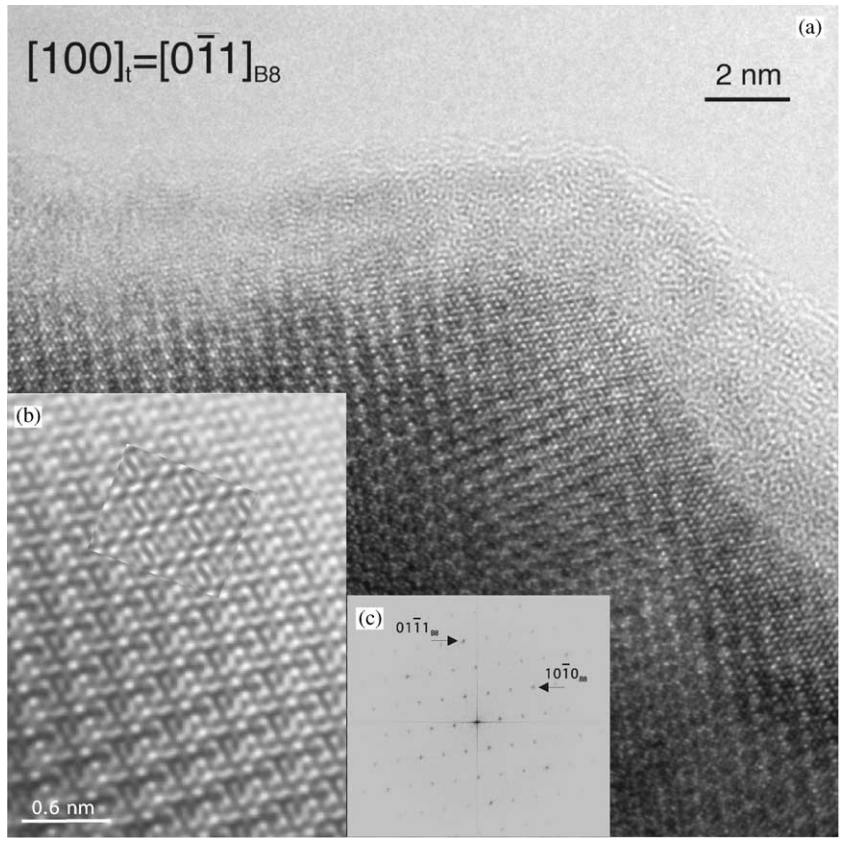

FIG. 5. (a) High-resolution electron microscopy image along $[0\bar{1}1]_{B8} = [100]_t$. This is the same direction as the EDP in Fig. 1a and the structure sketches in Fig. 3. (b) A filtered, averaged, enlarged area of the thinnest part of the crystal. The corresponding simulated image with a defocus of −450 Å and thickness of 20 Å is the inset. (c) The Fourier transform of the original image.

structure is a result of Sn and P atoms ordering on the hcp array coupled to Ni ordering in $\frac{1}{4}$ of the trigonal bipyramidal sites. Atoms coordinating the extra Ni atoms in the trigonal bipyramidal site define distorted Ni centered 11-vertex Edshammar polyhedra. All atoms in the structure belong to the Edshammar polyhedra and a building unit formed of two face-sharing Edshammar polyhedra can be used to describe the structure. This unit is spread over the structure via corner sharing in a rather peculiar fashion.

ACKNOWLEDGMENTS

Financial support from the Swedish Natural Science Council (NFR) is gratefully acknowledged. The authors thank Dr. Lasse Eriksson, Prof. Sven Lidin, and Dr. Simon Bennett at Stockholm University. "Luis Bru" electron microscopy center, Universidad Complutense de Madrid, is thanked for the facilities.

REFERENCES

1. A. Kjekshus and W. B. Pearson, *Prog. Solid State Chem.* **1,** 83 (1964).
2. A. K. Larsson, R. L. Withers, and L. Stenberg, *J. Solid State Chem.* **127,** 222–230 (1996).
3. A.-K. Larsson, L. Stenberg, and S. Lidin, *Acta Crystallogr. B* **50,** 636–643 (1994).
4. A.-K. Larsson, L. Stenberg, and S. Lidin, *Z. Kristallogr.* **210,** 832–837 (1995).
5. A. K. Larsson and R. L. Withers, *J. Alloys Compds.* **264,** 125–132 (1998).
6. A. G. Christy and A.-K. Larsson, *J. Solid State Chem.* **135,** 269–281 (1998).
7. A. G. Christy and A.-K. Larsson, *J. Solid State Chem.* **140,** 402–416 (1998).
8. O. N. Il'nitskaya, Yu B. Kuz'ma, and US Fundamenskii, *DNUND A* **1,** 79–81 (1989).
9. O. N. Il'nitskaya and Yu B. Kuz'ma, *Russ. J. Inorg. Chem.* **35**(8), 1104–1105 (1990).
10. O. N. Il'nitskaya, Yu N. Grin', and Yu B. Kuz'ma, *Kristallografiya* **37,** 141–150 (1991).
11. S. V. Orishchin and Yu B. Kuz'ma, *Inorg. Mater. (USSR)* **31**(3), 423–425 (1995).
12. R. Vincent and S. F. Pretty, *Philos Mag A* **53**(6), 843–862 (1986).
13. S. Furuseth and H. Fjellvåg, *Acta Chem. Scand. A* **39,** 537 (1985).
14. S. Furuseth and H. Fjellvåg, *Acta Chem. Scand. A* **48,** 134–138 (1994).
15. S. Furuseth, A.-K. Larsson, and R. L. Withers, *J. Solid State Chem.* **136,** 125–133 (1998).
16. W. Kaus and G. Nolze, "PowderCell 2. 1." Federal Institute for Materials and Testing Rudower Chaussee 5, 12489 Berlin, Germany, 1996.
17. P. E Werner, *Ark. Kemi* **31,** 513–516 (1969).
18. S. Hovmöller, *Ultramicroscopy* **41,** 121–135 (1992).
19. R. Kilaas, "45th Annual Proceedings of the Electron Microscopy Society of America, Baltimore, Maryland, p. 66," 1987.
20. Anonymous, "X-Shape: Crystal Optimisation for Numerical Absorption Correction." STOE& Cie GmbH, Hilperstrasse 10, D-64295, Darmstadt, Germany, 1996.
21. Anonymous, "X-red: STOE Data Reduction Program." STOE& Cie GmbH, Hilperstrasse 10, D-64295, Darmstadt, Germany, 1996.
22. G. M. Sheldrick, "SHELXS97. Program for the Solution of Crystal Structure." University of Göttingen, Germany, 1997.
23. C. Petricek, and M. Dusek, "The Crystallographic Computing System JANA2000." Insitute of Physics, Praha, Czech Republic, 2000.
24. J. P. Morniroli and J. W. Steeds, *Ultramicroscopy* **45,** 219–239 (1992).
25. L. E. Edshammar, "X-ray Studies on Binary Alloys of Aluminium with Platinum Metals." Ph.D. Thesis, University of Stockholm, 1969.
26. B. Hyde and S. Andersson, "Inorganic Crystal Structures." Wiley, New York, 1989.
27. W. Tremel, R. Hoffmann, and J. Silvestre, *J. Am. Chem. Soc.* **108,** 5174–5187 (1986).